

Relativistic chaotic scattering

Juan D. Bernal,^{1,*} Jesús M. Seoane,¹ and Miguel A.F. Sanjuán^{1,2,3}

¹*Nonlinear Dynamics, Chaos and Complex Systems Group,
Departamento de Física, Universidad Rey Juan Carlos,
Tulipán s/n, 28933 Móstoles, Madrid, Spain*

²*Department of Applied Informatics, Kaunas University of Technology,
Studentu 50-415, Kaunas LT-51368, Lithuania*

³*Institute for Physical Science and Technology,
University of Maryland, College Park, Maryland 20742, USA*

(Dated: August 23, 2018)

Abstract

The phenomenon of chaotic scattering is very relevant in different fields in science and engineering, and it has been mainly studied in the context of Newtonian mechanics. In this chapter, we study the chaotic scattering considering the special relativity, not just for high velocities but also small ones. We indeed research on global properties of any chaotic scattering system as the escape time distribution and the decay law. Moreover, we study some relevant characteristics of the system exit basin topology as the uncertainty dimension, the Wada property and the basin entropy. As a prototypical chaotic scattering model, we use the relativistic Hénon-Heiles Hamiltonian. Our results show that the average escape time decreases with increasing values of the relativistic factor β . We have found a cross-over point for which the KAM islands in the phase space are destroyed when $\beta \simeq 0.4$. The study of the survival probability of the particles in the scattering region shows an algebraic decay for values of $\beta \leq 0.4$, and this law becomes exponential for $\beta > 0.4$. A scaling law between the exponent of the decay law and the β factor is uncovered. With regards to the exit basin topology, our main findings for the uncertainty dimension show two different behaviors insofar we change the relativistic parameter β . These are related with the disappearance of KAM islands in phase space. Moreover, the computation of the exit basins in the phase space suggests the existence of Wada basins for $\beta > 0.625$. We have also studied the evolution of the exit basins by computing the basin entropy. It shows a maximum value for $\beta \approx 0.2$. Our work might be relevant to galactic dynamics and it also has important applications as, for example, in the Störmer problem.

PACS numbers: 05.45.Ac,05.45.Df,05.45.Pq

* juandiego.bernal@urjc.es

I. INTRODUCTION

Chaotic scattering in open Hamiltonian systems has been a broad area of study in nonlinear dynamics, with applications in numerous fields in physics (see Refs. [1, 2]). This topic is essentially defined by a *scattering region* where there are interactions between incident particles and a potential. Outside this region the influence of the potential on the particles is negligible and the motions of the incident particles are uniform. For many applications of physical interest, the equations of motion of the test particles are nonlinear and the resultant dynamics is chaotic in the scattering region. Therefore, slightly similar initial conditions may describe completely different trajectories. Since the system is open, this region possesses exits for which the particles may enter or escape. Quite often, particles starting in the scattering region bounce back and forth for a finite time before escaping. In this sense chaotic scattering could be presented as a physical manifestation of transient chaos ([3, 4]).

Using the Newtonian approximation for modeling the dynamics of the system is the most widely accepted convention in physics and engineering applications when the speed of objects is low compared to the speed of light [5]. Nevertheless, if the dynamics of the system is really sensitive to the initial conditions, the trajectories predicted by the Newtonian scheme rapidly disagree with the ones described by the special relativity theory (see Refs. [6–9]). Recently, there have been some results ([10]) that pointed out that the global properties of the dynamical systems, such as the dimension of the nonattracting chaotic invariant set, are more robust and the Newtonian approximation actually provides accurate enough results for them in slow chaotic scattering motion. The first goal of this chapter is to show that there are relevant global properties of chaotic scattering systems that indeed do depend on the effect of the Lorentz transformations and we may consider the special relativity scheme in case we want to describe them in a realistic manner, even for low velocities. Specifically, we focus our study in both the average escape times and in the decay law of the particles from the scattering region which are quite important global properties in the scattering systems. These results were presented in Ref. [11]. Furthermore, we analyze in detail some key properties that characterized the exit basin topology of this kind of systems: the uncertainty dimension, the Wada property and the basin entropy. This is important since the exit basin topology is useful to achieve a priori very rich global insights. For example, once we know the exit basin topology of a system, we can infer the degree of unpredictability of the final state

of the system by just knowing some approximate information about the initial conditions. The research over the exit basin topology is published in Ref. [12].

The authors of the present work showed in the past the effect of external perturbations as noise and dissipation in some Hamiltonian systems (see for example Ref. [13]). It is worth highlighting that the consideration of the relativistic framework on the system dynamics cannot be considered as an external perturbation like the noise or the dissipation, although the global properties of the system also change.

From now on, we will refer to relativistic to any effect where the Lorentz transformations have been considered. Likewise, we say that any property or object is nonrelativistic or Newtonian when we do not take into consideration the Lorentz transformations but the Galilean ones.

This chapter is organized as follows. In Sec. II, we describe our prototype model, the relativistic Hénon-Heiles system. The effects of the Lorentz transformation on the average escape time of the particles and their decay law are carried out in Sec. III. In Sec. IV, we give an heuristic reasoning based on energetic considerations to explain the results obtained for both global properties. Moreover, here we characterize the decay law of the relativistic particles. In Sec. V, we show the effects of the Lorentz transformation on the uncertainty dimension of a typical scattering function. A qualitative description of the influence of the special relativity in the exit basins is shown in Sec. VI. Additionally, we use the basin entropy to quantify the uncertainty of the system based on the study of the exit basin topology. Then, we understand the different sources of uncertainty in the relativistic Hénon-Heiles system provoked by the Lorentz transformations. A discussion and the main conclusions of this chapter are presented in Sec. VIII.

II. MODEL DESCRIPTION

We focus our study on the effects of the relativistic corrections in a paradigmatic chaotic scattering system, the Hénon-Heiles Hamiltonian. The two-dimensional potential of the Hénon-Heiles system is defined by

$$V(x, y) = \frac{1}{2}k(x^2 + y^2) + \lambda(x^2y - \frac{1}{3}y^3). \quad (1)$$

We consider the Hénon-Heiles potential in a system of units where $k = \lambda = 1$, see Ref. [14]. Its isopotential curves can be seen in Fig. 1. Due to the triangular symmetry of the system, the exits are separated by an angle of $2\pi/3$ radians. We call Exit 1 the upper exit ($y \rightarrow +\infty$), Exit 2, the left one ($y \rightarrow -\infty, x \rightarrow -\infty$), and, Exit 3, the right exit ($y \rightarrow -\infty, x \rightarrow +\infty$).

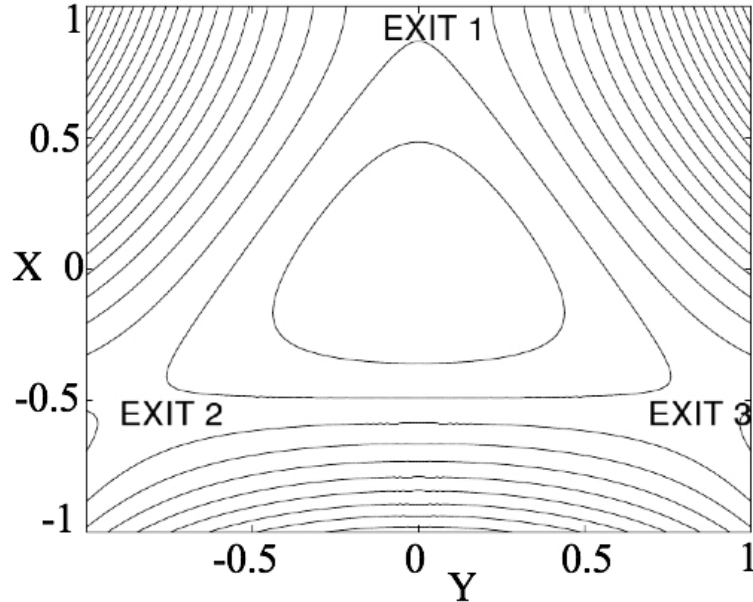


FIG. 1. **Isopotential curves for the Hénon-Heiles potential:** they are closed for energies below the nonrelativistic threshold energy escape $E_e = 1/6$. It shows three different exits for energy values above $E_e = 1/6$.

We define the nonrelativistic total mechanical energy and we call it *Newtonian energy*, E_N , as $E_N = T(\mathbf{p}) + V(\mathbf{r})$, where T is the kinetic energy of the particle, $T = \mathbf{p}^2/2m$, \mathbf{p} is its linear momentum vector, $V(\mathbf{r})$ is the potential energy, and \mathbf{r} its vector position. If $E_N \in [0, 1/6]$, the trajectory of any incident particle is trapped in the scattering region. For $E_N > 1/6$, the particles may eventually escape up to infinity. There are indeed three different regimes of motion depending on the initial value of the energy: (a) closed-nonhyperbolic $E_N \in [0, 1/6]$, (b) open-nonhyperbolic $E_N \in (1/6, 2/9)$ and (c) open-hyperbolic $E_N \in [2/9, +\infty)$ [15]. In the first energy range, all the trajectories are trapped and there is no exit by which any particle may escape. When $E_N \in (1/6, 2/9)$, the energy is large enough to allow escapes from the scattering region and the coexistence of stable invariant tori with chaotic saddles, which typically results in an algebraic decay in the survival probability of a particle in the scattering region. On the contrary, when $E_N \in [2/9, +\infty)$, the regime is open-hyperbolic and all the periodic trajectories are unstable;

there is no KAM tori in phase space.

If we consider the motion of a relativistic particle moving in an external potential energy $V(\mathbf{r})$, the Hamiltonian (or the total energy) is:

$$H = E = \gamma mc^2 + V(\mathbf{r}) = \sqrt{m^2 c^4 + c^2 \mathbf{p}^2} + V(\mathbf{r}), \quad (2)$$

where m is the particle's rest mass, c is the speed of light and γ is the Lorentz factor which is defined as:

$$\gamma = \sqrt{1 + \frac{\mathbf{p}^2}{m^2 c^2}} = \frac{1}{\sqrt{1 - \frac{v^2}{c^2}}}. \quad (3)$$

Therefore, the Hamilton's canonical equations are:

$$\begin{aligned} \dot{\mathbf{p}} &= -\frac{\partial H}{\partial \mathbf{r}} = -\nabla V(\mathbf{r}), \\ \dot{\mathbf{r}} = \mathbf{v} &= \frac{\partial H}{\partial \mathbf{p}} = \frac{\mathbf{p}}{m\gamma}, \end{aligned} \quad (4)$$

When $\gamma = 1$ the Newtonian equations of motion are recovered from Eq. 4. We define β as the ratio v/c , where v is the modulus of the vector velocity \mathbf{v} . Then the Lorentz factor can be rewritten as $\gamma = \frac{1}{\sqrt{1-\beta^2}}$. Whereas $\gamma \in [1, +\infty)$, the range of values for β is $[0, 1]$. However, γ and β express essentially the same: how large is the velocity of the object as compared to the speed of light. From now on, we will use β instead of γ to show our results for mere convenience.

Taking into consideration Eqs. 1 and 4, the relativistic equations of motion of a scattering particle of unit rest mass ($m = 1$) interacting with the Hénon-Heiles potential are:

$$\begin{aligned} \dot{x} &= \frac{p}{\gamma}, \\ \dot{y} &= \frac{q}{\gamma}, \\ \dot{p} &= -x - 2xy, \\ \dot{q} &= -y - x^2 + y^2, \end{aligned} \quad (5)$$

where p and q are the two components of the linear momentum vector \mathbf{p} .

In the present work, we aim to isolate the effects of the variation of the Lorentz factor γ (or β as previously shown) from the rest of variables of the system, *i.e.*, the initial velocity of the particles, its energy, etc. For this reason, during our numerical computations we have used a different systems of units so that γ be the only varying parameter in the equations of motion (Eq. 5).

Therefore, we analyze the evolution of the properties of the system when β varies, by comparing these properties with the characteristics of the nonrelativistic system. Then we have to choose the same value of the initial velocity, $v = 0.583$, in different systems of units. This initial velocity corresponds to a Newtonian energy $E_N = 0.17$, which is in the open-nonhyperbolic regime and quite close to the limit E_e . For the sake of clarity, we consider an incident particle coming from the infinity to the scattering region. Then, imagine that we measure the properties of the incident particle in the system of Planck units. In this system, the speed of light is $c = 1 c$, that is, the unit of the variable speed is measured as a multiple of the speed of light c instead of, for instance, in m/s . Now, suppose that, according to our measures, the rest mass of the particle is $m = 1 m_P$ (in the Planck units, the mass is expressed as a multiple of the Planck mass m_P , which is $m_P \approx 2.2 \times 10^{-8} kg$). Likewise, the speed of the particle is $v = 0.583 c$. According to the Newtonian scheme, the classical energy of the particle is $E_N = \frac{1}{2}v^2 \approx 0.17 E_P$, where E_P is the Planck energy, which is the energy unit in the Planck units system ($E_P \approx 1.96 \times 10^9 J$). Now, we consider another incident particle with different rest mass and velocity, however we choose the International System of Units (*SI*) to measure its properties. In this case, we obtain that its rest mass is again the unity, although now the rest mass is one kilogram, $m = 1 kg$, and its velocity is $v = 0.583 m/s$. The speed of light in *SI* is $c \approx 3 \times 10^8 m/s$. The initial Newtonian energy of the particle is $E_N \approx 0.17 J$ in *SI*, but now the initial velocity is almost negligible as compared to the speed of light, that is, $\beta = v/c = 0.583/3 \times 10^8 \approx 2 \times 10^{-9}$. Therefore, from the perspective of the equations of motion of both particles, when we just consider the Galilean transformations, we can conclude that the behavior of the particles will be the same since $V(x, y)$ of Eq. 1 is equal in both cases, as long as the parameters $k = \lambda = 1$ in their respective system of units. However, they are completely different when the relativistic corrections are considered because the Lorentz factor γ affects the equations of motion by the variation of β , regardless the chosen system of units. To summarize, the objective of our numerical computations and analysis is to study the effect of γ in the equations of motion, so the key point is to set the speed of light c as the threshold value of the speed of the particles, regardless the system of units we may be considering. We represent Fig. 2 in order to give a visual example about the effect of the Lorent factor in the evolution of single trajectories. There, we represent three different trajectories of the same relativistic particle when it is shot at the same initial Newtonian velocity, $v = 0.583$, from the same initial conditions, $x = 0$, $y = 0$ and equal initial shooting angle $\phi = 0.8\pi$. However, that velocity, measured in different systems of units, represents different values of the parameter β . Fig. 2(a) is the trajectory of the

particle for $\beta = 0.01$. The particle leaves the scattering region by Exit 1 at 286,56 seconds. In Fig. 2(b) we represent the trajectory for $\beta = 0.1$. The particle is trapped in the scattering region forever. Fig. 2(c) shows the trajectory of the particle for $\beta = 0.8$. It leaves the scattering region by Exit 3 in 18,19 seconds. We can see that, even for low velocities the trajectories described for the particles are completely different.

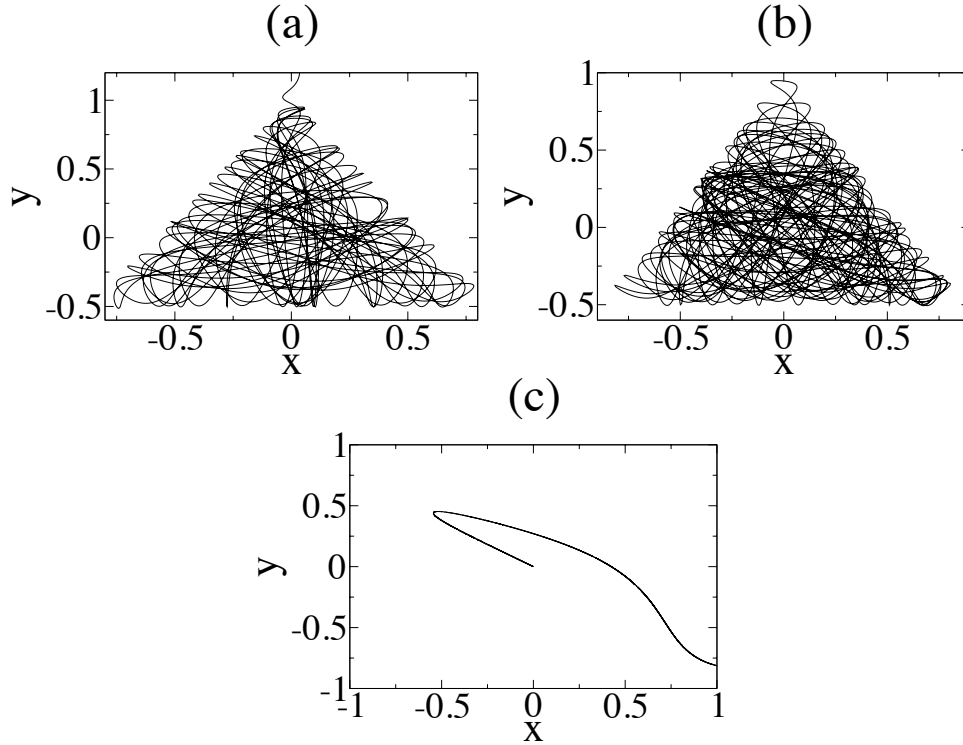


FIG. 2. Single trajectories for relativistic particles in the scattering region. It shows different trajectories of the same relativistic particle when it is shot at the same initial Newtonian velocity, $v = 0.583$, from the same initial conditions: $x = 0$, $y = 0$ and shooting angle $\phi = 0.1\pi$. That velocity is measured in different systems of units, representing different values of the parameter β . (a) is the trajectory of the particle for $\beta = 0.01$. The particle leaves the scattering region by Exit 1 at 286,56 seconds. (b) represents the trajectory for $\beta = 0.1$. The particle is trapped in the scattering region forever. (c) shows the trajectory of the particle for $\beta = 0.8$. It leaves the scattering region by Exit 3 in 18,19 seconds.

III. NUMERICAL RESULTS ON THE ESCAPE TIME AND THE DECAY LAW

Here we study the discrepancies between the relativistic and the nonrelativistic corrections when we analyze the *average escape time*, \bar{T}_e , of the system. Furthermore, we analyze another fundamental piece of any chaotic scattering system, its time delay statistics $P(t)$ when we consider the Lorentz corrections. Both are essential global characteristics in chaotic scattering problems.

A. Escape time

The *escape time*, T_e , of an incident particle is defined as the time spent by it in the scattering region. For times above T_e , the particle travels to infinity after having crossed one of the three exit boundaries, which are extremely unstable trajectories called *Lyapunov orbits* (see Ref. [16]). In the case of the Hénon-Heiles system, the Lyapunov trajectories exist for energies higher than $E_e = 1/6$. The higher the energy, the shorter the escape times are. When we consider a large number of particles and we average their individual T_e , then we obtain the global property \bar{T}_e , which is a unique and characteristic property of the system. We represent in Fig. 3 the average escape time, \bar{T}_e , of 10,000 particles shot inside the scattering region with an initial velocity $v = 0.583$. The initial conditions are $(x_0, y_0, \dot{x}_0, \dot{y}_0) = (0, 0, v \cos(\varphi), v \sin(\varphi))$, with shooting angle, $\varphi \in [0, 2\pi]$. We use 500 different values of β for our calculations. The Newtonian average escape time in Fig. 3 is the first point of the graph, when $\beta \rightarrow 0$. This value is indeed the inner average escape time of the particles. As a reminder, this is the time as seen by an observer who is stationary with regard to the reference frame of the particle. Then, if we average the measures of the inner escape time of the 10,000 particles, then we get the value of \bar{T}_e when $\beta \rightarrow 0$. As can be seen in Fig. 3, there is a clear influence of the Lorentz factor variation on the average escape time \bar{T}_e . It is worth to note that, in the most general sense, we define scattering as the problem of obtaining the relationship between an *input* variable taken from outside the scattering region and an *output* variable, which characterizes the final state of the system after interacting with the scattering region. However, the fact of starting the numerical experiments inside the scattering region is a convention frequently used in the scientific literature (see for example Refs. [17–19]). The reason behind this is to take advantage of the well-known topological structure of the escape basins resulting from the Poincaré surface of section (\dot{y}, y) for $x(0) = 0$. Therefore it is implicitly assumed that the initial conditions chosen for the computations may correspond to trajectories which come from outside the scat-

tering region and, after bouncing back and forth for a certain time in the scattering region, they pass through $x = 0$ with a certain velocity (\dot{x}, \dot{y}) . This is the precise instant when the simulations start and the initial conditions are set as $(x = 0, y, \dot{x}, \dot{y})$. According to Fig. 3, there is a relevant decrease of \bar{T}_e up to $\beta \approx 0.4$. Indeed at $\beta \approx 0.4$ there is a leap where the linear decrease trend of \bar{T}_e changes abruptly. This can be explained when we highlight that at $\beta \approx 0.4$ the KAM islands are almost destroyed and there are just a few trajectories trapped in the scattering region forever. In fact, as it has been shown in the literature [20], the KAM islands exhibit certain stickiness in the sense that its presence in the phase space provokes longer transients inside the scattering region. In order to confirm the destruction of the KAM island at $\beta \approx 0.4$, we analyze in Fig. 4 the percentage, expressed as a decimal, of particles trapped in the scattering region at t_{max} . We name this percentage ϕ_{KAM} and it is directly related to the presence of KAM islands and its Lebesgue measure in the Poincaré surface of section.

To calculate Φ_{KAM} we have considered again 10,000 particles inside the scattering region with initial conditions $(x_0, y_0, \dot{x}_0, \dot{y}_0) = (0, 0, 0.583 \cos(\varphi), 0.583 \sin(\varphi))$ and shooting angle $\varphi \in [0, 2\pi]$. Then we compare the number of particles remaining in the scattering region after a long transient, t_{max} , with the total number of the initially shot particles, obtaining the quantity Φ_{KAM} for a certain value of β . Finally, we take different values of β and we represent Φ_{KAM} vs β to get Fig. 4. The results point out that, even for low velocities ($\beta < 0.2$) the number of trapped particles decreases as β increases. When $\beta \approx 0.4$ there are almost no particles trapped in the scattering region, which is a direct proof of the destruction of the KAM islands. It is worth noting that the shape of both curves, $\bar{T}_e(\beta)$ and $\Phi_{KAM}(\beta)$, as shown in Figs. 3 and 4, are very similar, which expresses the relevance of the KAM destruction mechanism over the global properties of the system.

In Sec. IV we will discuss the reasons behind the trend of the average escape time \bar{T}_e of the system under the variation of β from Fig. 3.

B. Decay law

Suppose that we pick many different initial conditions at random in some interval of the domain. Then we examine the resulting trajectory for each value and determine the time t that its trajectory spends in the scattering region. The fraction of trajectories with *time delay* between t and $t + dt$ is $P(t)dt$. For open nonhyperbolic dynamics with bounding KAM surfaces in the scattering region, one finds that for large t the time delay statistics, $P(t)$, decays algebraically as

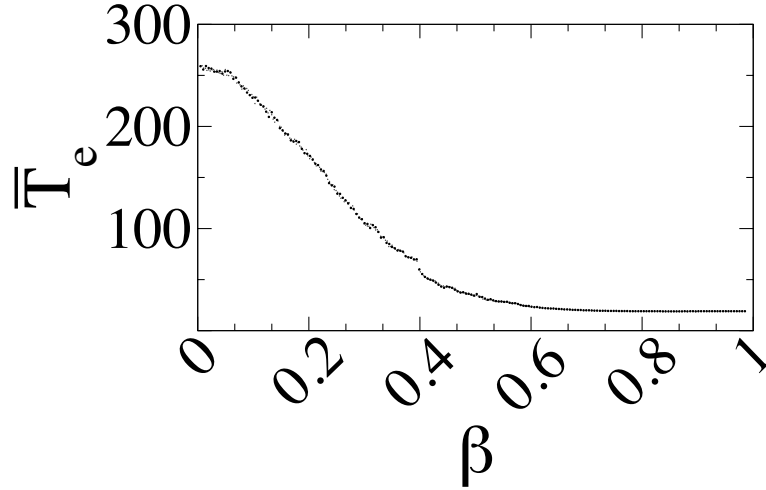


FIG. 3. **Average escape time:** \bar{T}_e of 10,000 particles inside the scattering region with initial velocity $v = 0.583$. The initial conditions are $(x_0, y_0, x'_0, y'_0) = (0, 0, v \cos(\varphi), v \sin(\varphi))$, with shooting angle, $\varphi \in [0, 2\pi]$. We use 500 different values of β in our calculations. There is a linear decrease of \bar{T}_e up to $\beta \approx 0.4$. Indeed at $\beta \approx 0.4$ there is a leap where the linear decrease trend of \bar{T}_e changes abruptly. Figure obtained from Ref. [11].

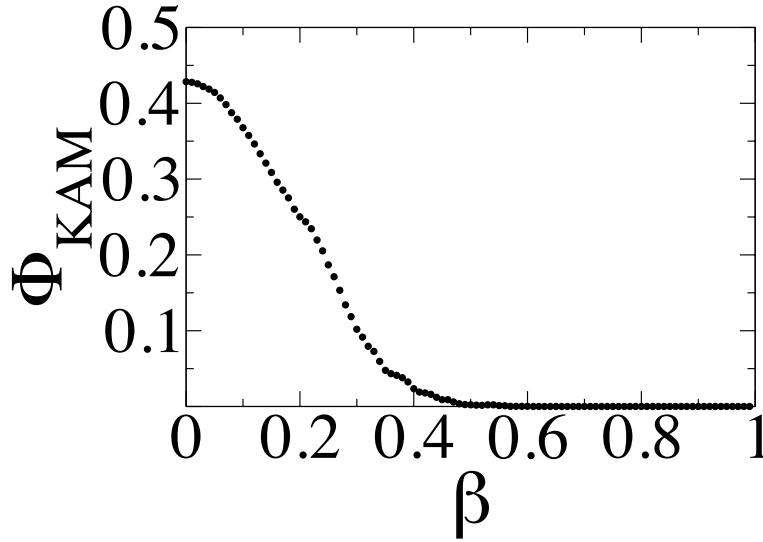


FIG. 4. **Percentage of trapped particles in the scattering region:** Φ_{KAM} , expressed as a decimal, at t_{max} , is directly proportional to the Lebesgue measure of the KAM islands in the Poincaré surface of section. At $\beta \approx 0.4$ there are just a few particles trapped in the scattering region. Figure obtained from Ref. [11].

follows,

$$P(t) \sim t^{-\alpha}. \quad (6)$$

An algebraic decay law as the described in Eq. 6 is also found in higher dimensional Hamiltonian systems when the phase space is partially filled with a KAM tori (see Ref. [21]).

For our simulations we have considered 10,000 particles shot inside the scattering region with initial velocities $v \approx 0.5831$. The initial conditions are $(x_0, y_0, \dot{x}_0, \dot{y}_0) = (0, 0, v \cos(\varphi), v \sin(\varphi))$, with shooting angle, $\varphi \in [0, 2\pi]$. Then we get the fraction of particles inside the scattering region between t and $t + dt$, that is $P(t)dt$, and we represent $\log_{10}(P(t))$ vs. $\log_{10}(t)$ to get the value of the parameter α (the slope of the resulting straight line). Calculating α for different values of β , we obtain the evolution of the parameter α with β . In Fig. 5 we can see that the numerical values of $\alpha(\beta)$ fits a quadratic curve as $\alpha \approx A_0 + A_1\beta + A_2\beta^2$ with $A_0 = 0.46138$, $A_1 = -2.5311$ and $A_2 = 15.185$. We have indeed found that the decay law of the time delay statistics is algebraic, according to Eq. 6, for the range of energies where the regime of the system is open nonhyperbolic. For the initial conditions chosen to perform our computations, this regime takes up to $\beta \approx 0.4$. The value of the coefficients A_0 , A_1 and A_2 are exclusively valid in the range of values that we have considered for the nonlinear fitting, $[0.05, 0.4]$. However, we can expect that the value of the parameter α in the nonrelativistic framework may be similar to the one obtained by the quadratic formula. That is because the minimum value of the range considered for the fitting, that is 0.05, is relatively close to $\beta \rightarrow 0$. Indeed, the coefficient $A_0 = 0.461$ may be deemed as a good approximation of the Newtonian framework since this yields a value for α equals to 0.386.

As the speed of particles increases and $\beta > 0.4$, the measure of bounding KAM surfaces is practically negligible in the scattering region and all the trajectories exit from there. The decay law of the particles becomes exponential according to Eq. 7:

$$P(t) \sim e^{-\tau t}, \quad (7)$$

where $1/\tau$ is the characteristic time for the scatterer.

We can proceed similarly to calculate the evolution of the parameter τ while β is increased. We shoot 10,000 particles inside the scattering region with initial conditions are $(x_0, y_0, \dot{x}_0, \dot{y}_0) =$

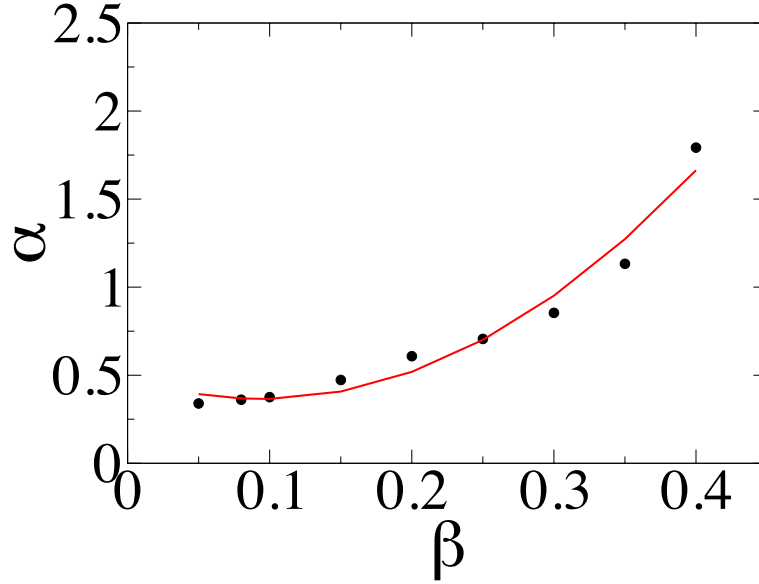


FIG. 5. (Color online) **Evolution of the parameter α** : we show the exponent α of the algebraic decay law (see Eq. 6) in the relativistic Hénon-Heiles system under the variation of β . The initial velocity of $v \approx 0.5831$. There is a quadratic trend, $\alpha \approx A_0 + A_1\beta + A_2\beta^2$, where $A_0 = 0.46138$, $A_1 = -2.5311$ and $A_2 = 15.185$. Figure obtained from Ref. [11].

$(0, 0, v \cos(\varphi), v \sin(\varphi))$, with $v \approx 0.5831$ and shooting angle, $\varphi \in [0, 2\pi]$. Getting the fraction of particles inside the scattering region between t and $t + dt$, we represent $\ln(P(t))$ vs. t . The slope of the resulting straight line is the value of the parameter τ . If we do the same for increasing values of β we obtain the relation between τ and β . In Fig. 6 is shown the quadratic evolution of the numerical data of the parameter τ while the Lorentz factor varies according to $\tau \approx \tau_0 + \tau_1\beta + \tau_2\beta^2$, where $\tau_0 = 0.065207$, $\tau_1 = -0.028988$ and $\tau_2 = 0.4125$.

In the next section we will see why the numerical values of $\alpha(\beta)$ and $\tau(\beta)$ follow a quadratic trend.

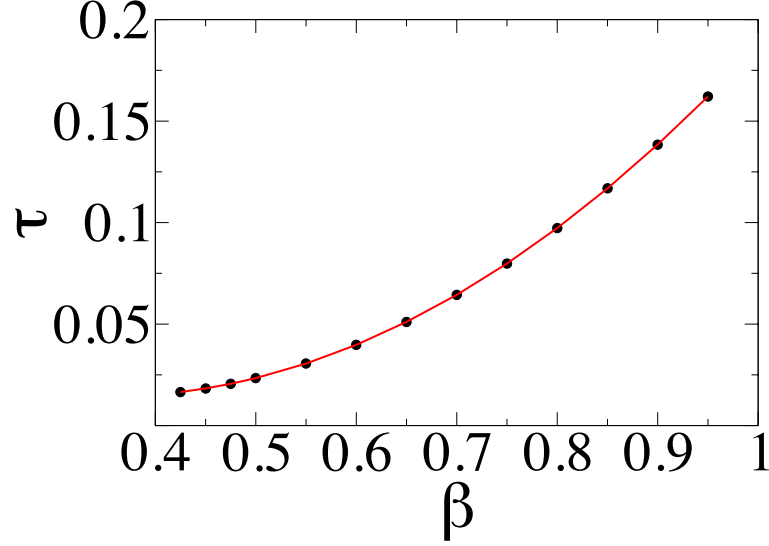


FIG. 6. (Color online) **Evolution of the parameter τ :** of the exponential decay law of the relativistic Hénon-Heiles system under the variation of β . The initial velocity of $v \approx 0.5831$. The trend is quadratic, $\tau \approx \tau_0 + \tau_1\beta + \tau_2\beta^2$, where $\tau_0 = 0.065207$, $\tau_1 = -0.028988$ and $\tau_2 = 0.4125$. Figure obtained from Ref. [11].

IV. DISCUSSION ABOUT THE ESCAPE TIME AND THE DECAY LAW

A. Energetic reasoning about the escape time and the decay law

In the present section we follow a qualitative approach to discuss the trends of the global properties of the system that we have studied in Secs. III A and III B as $\bar{T}_e(\beta)$, $\alpha(\beta)$ and $\tau(\beta)$.

Firstly we take the relativistic kinetic energy of the system, $K = m\gamma c^2 - mc^2$, as a explicit function of β :

$$K(\beta) = \frac{v^2}{\beta^2 \sqrt{1 - \beta^2}} - \frac{v^2}{\beta^2}. \quad (8)$$

In Fig. 7 we represent $K(\beta)$. If we try to fit the curve $K(\beta)$ to a polynomial while the system is in the open nonhyperbolic regime (up to $\beta \approx 0.4$), we see that the numerical values of the relativistic kinetic energy of the system fit a quadratic curve: $K(\beta) \approx K_0 + K_1\beta + K_2\beta^2$, where $K_0 = 0.25676$, $K_1 = -0.77133$ and $K_2 = 1.2553$.

The parameter α of Eq. 6 is related to the square of the average speed by which the particles leave the scattering region. The higher the α , the faster decays $P(t)$ and, therefore, the quicker the

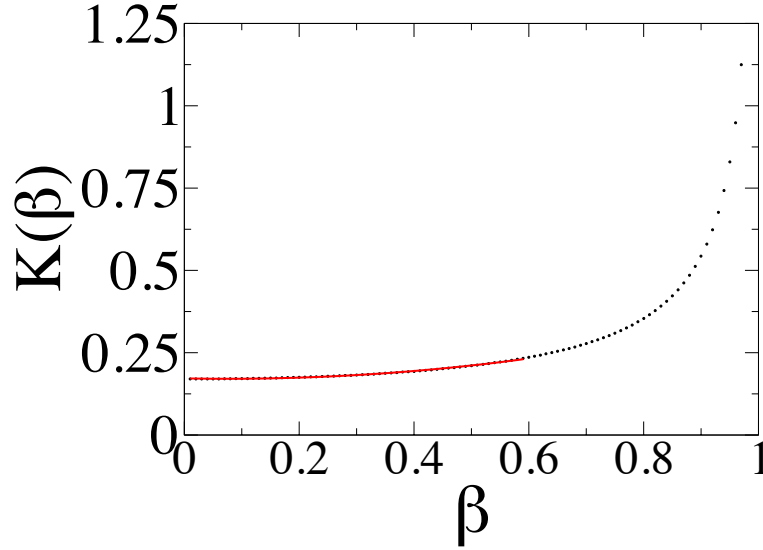


FIG. 7. (Color online) **Representation of the relativistic kinetic energy:** of the system as a explicit function of β , $K(\beta)$ (see Eq. 8). While the system is in the open nonhyperbolic regime, the kinetic energy fits a quadratic curve. $K(\beta) \approx K_0 + K_1\beta + K_2\beta^2$, where $K_0 = 0.25676$, $K_1 = -0.77133$ and $K_2 = 1.2553$. Figure obtained from Ref. [11].

particles exit from the scattering region. Therefore, we may consider that the parameter α should be directly proportional to the energy of the system, in a linear way. This is indeed the case of the nonrelativistic Hénon-Heiles system. In Fig. 8 we show the linear relation between the parameter α and the total energy of the classical Hénon-Heiles system, E_N , in the open nonhyperbolic regime. This numerical result was also demonstrated in previous works [22]. Then, if the energy of the system fits a quadratic curve of β and it is also directly proportional to α , we may expect that the parameter α shows a quadratic trend when β is varied.

As we have done for the open nonhyperbolic regime, now we can proceed to fit the curve $K = K(\beta)$ to a quadratic curve, while the system is in the open hyperbolic regime, $\beta \in (0.4, 0.8]$. This is shown in Fig. 8. It yields a second order curve $K(\beta) \approx K_0 + K_1\beta + K_2\beta^2$, where $K_0 = 0.254$, $K_1 = -0.3869$ and $K_2 = 5968$. $R^2 = 0.9971$. The goodness of the fit of the numerical data of $K = K(\beta)$ in the open hyperbolic regime to a quadratic curve is quite high so we can conclude that, within this regime of energy, $K \propto \beta^2$. The parameter τ of Eq. 7 is also related to the square of the average speed by which the particles leave the scattering region. Then we can again conclude that τ is linearly proportional to the energy of the system and, therefore, that explains why the numerical values of $\tau(\beta)$ follows a quadratic trend for the considered range

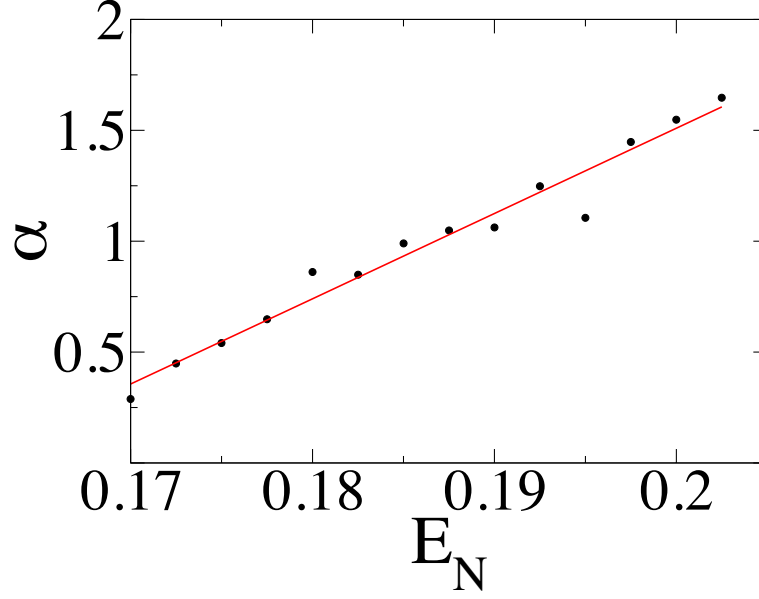


FIG. 8. (Color online) **Linear correlation between α and the total energy of the nonrelativistic Hénon-Heiles system. Figure obtained from Ref. [11].**

of β .

We are now in the position to understand the linear trend of the curve $\bar{T}_e(\beta)$ before the KAM island destruction at $\beta \approx 0.4$ as shown in Fig. 3. If $K \propto \alpha$ and $\alpha \propto \beta^2$, considering that β is a magnitude related to the velocity of the particles, and this is inversely proportional to the escape time, then $1/\bar{T}_e \propto \beta^2$. In Fig. 9, we can see the results obtained from our computations. The relation between $1/\bar{T}_e$ and β^2 is linear. The interesting result is that there has been detected a transition from $\beta \in [0, 0.4)$ (or $\beta^2 \in [0, 0.16)$ in the graph) to $\beta \in [0.4, 0.6]$ (or $\beta^2 \in [0.16, 0.40]$). This transition is corresponding to the destruction of the KAM tori (about $\beta \sim 0.4$). This explains the leap that can be seen in Fig. 3 at $\beta \sim 0.4$. This is also the value where the percentage of trapped particles turns sharply towards zero in Fig. 4. Both slopes of the straight lines of Fig. 9 determine the speed of the particles exiting from the scattering region. Then it is another numerical evidence of the KAM island stickiness.

Likewise, since $\tau \propto \beta^2$ according to Fig. 6 and we can again state that β is inversely proportional to the escape time, then $1/\bar{T}_e \propto \beta^2$. Therefore, the same reasoning can be used to explain the behavior of the Fig. 3 from $\beta \sim 0.4$ on.

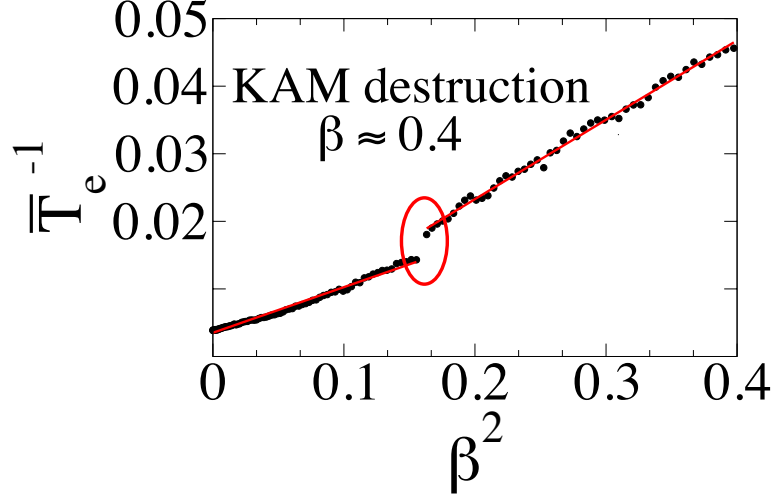


FIG. 9. (Color online) **Analysis of the relation between the average escape time of the particles \bar{T}_e and β :** we show the linear relation between $1/\bar{T}_e$ and β^2 . At $\beta \sim 0.4$ (that is, $\beta^2 \sim 0.16$ in the graph), we can see a transition corresponding to the destruction of the KAM tori. This explains the leap that can be seen in Fig. 3 at $\beta \sim 0.4$ and why the percentage of trapped particles in the scattering region turns sharply towards zero in Fig. 4. Figure obtained from Ref. [11].

B. Decay law characterization

In previous studies, Zhao and Du derived a formula for the exponential decay law, setting the parameter τ of Eq. 7 as a function of the energy of the nonrelativistic Hénon-Heiles system (see Ref. [22]). The regime of energies considered by them was the open hyperbolic one, simplifying the model with the assumption of the nonexistence of KAM islands for Newtonian energies higher than $E_N = 1/6$. In this section we apply a similar methodology for the open hyperbolic regime but considering the relativistic corrections in order to find a theoretical expression for the escape rate of the Hénon-Heiles system. The phase space distribution can be generally expressed as

$$\psi(p, q) = \frac{\delta(\Delta E - H(p, q))}{\int dpdq \delta(\Delta E - H(p, q))}, \quad (9)$$

where p and q are the coordinates of the linear momentum (see Ref. [23]). δ is the operator that expresses a small variation of the variables in brackets. ΔE is the difference between the relativistic mechanical energy, $K + V = E - mc^2$, and the threshold energy where the whole phase space of the system is chaotic and the particles may escape from the scattering region, $E_e = 1/6$. For convenience and simplicity, we have selected $K + V$ instead of the total relativistic

energy E in the following calculations. In fact, the constant value of ΔE equals the kinetic energy of the particle when it is freely moving outside the scattering region according to Eq. 8. When it is under the effect of the Hénon-Heiles potential V , then the kinetic and the potential energy are continually being exchanged in order to keep constant the sum $K + V$. ΔE is a conserved quantity and the following reasoning is completely valid. The phase space distribution can be rewritten in terms of (x, y, θ) as $\rho(x, y, \theta) = \frac{1}{2\pi S(\Delta E)}$, where θ is the angle between the direction of the momentum \mathbf{p} and the y axis. $S(\Delta E)$ is the area of the well. To define the area of the well, we have to consider the straight lines which contain the three saddle points of the Hénon-Heiles system and are perpendicular to the direction of the bisector lines of the equilateral triangle arranged by those three saddle points. Therefore, S is the region bounded by the well contour lines and the aforesaid straight lines. Given N particles in the S region, the number of particles leaving the well through the opening at a saddle point (for instance, $P_1 = (0, 1)$) in a unit time can be expressed as $N \int_{x_A}^{x_B} dx \int_{-\pi/2}^{\pi/2} \rho(x, y, \theta) v(x, y) \cos(\theta) d\theta$, where the integral in x is along the straight line which contains P_1 . The limits of integration x_A and x_B are the points where the contour lines of the Hénon-Heiles potential intersect the straight line that contains P_1 . If we note the triangular symmetry of the system, the number of particles leaving the well in a unit time from the three openings are just three times the previous result. The change of N with respect to t is

$$\frac{dN(t)}{dt} = -3N(t)\rho \int_{-\pi/2}^{\pi/2} \cos(\theta) d\theta \int_{-\sqrt{2\Delta E/3}}^{\sqrt{2\Delta E/3}} \sqrt{2(\Delta E - 3x^2/2)} dx = -2\pi\sqrt{3}\Delta E\rho N(t). \quad (10)$$

If we compare this result with the Eq. 7, we obtain the analytical expression for the escape rate as

$$\tau(\Delta E) = \frac{\sqrt{3}\Delta E}{S(\Delta E)}. \quad (11)$$

There is no algebraic approach to obtain the expression of $S = S(\Delta E)$, but we can determine it by applying an indirect method as, for instance, the Monte Carlo method. In Fig. 10(a) we represent the area of the well S as a function of ΔE . The numerical results fit a quadratic polynomial: $S(\Delta E) = S_0 + S_1\Delta E + S_2\Delta E^2$, with $S_0 = 1.299$, $S_1 = 6.7271$ and $S_2 = -7.3541$. The value S_0 is in fact the area of the equilateral triangle whose vertexes are the three saddle points of the Hénon-Heiles system, that is $S_0 = \frac{3\sqrt{3}}{4}$. Therefore, we can obtain the expression of $\tau = \tau(\Delta E)$ as

$$\tau(\Delta E) = \frac{\sqrt{3}\Delta E}{S_0 + S_1\Delta E + S_2\Delta E^2}. \quad (12)$$

In Fig. 10(b) we show S as a function of β . Again the numerical results fit a quadratic relation: $s(\beta) = s_0 + s_1\beta + s_2\beta^2$, with $s_0 = 2.2321$, $s_1 = -3.7433$ and $s_2 = 4.8112$.

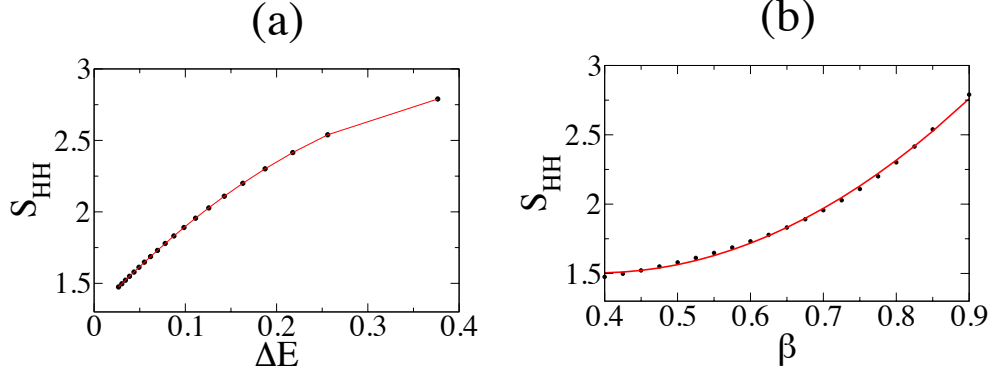


FIG. 10. (Color online) **Area of the well S of the Hénon-Heiles system:** in panel (a) we show the evolution of S under the variation of energy of the system ΔE . The initial velocity is $v \approx 0.5831$. The trend is quadratic, $S(\Delta E) = S_0 + S_1\Delta E + S_2\Delta E^2$, with $S_0 = 1.299$, $S_1 = 6.7271$ and $S_2 = -7.3541$. The regime of considered energies is the hyperbolic one, from $\beta = 0.4$ on. The maximum value of the energy ΔE is the correspondent to $\beta = 0.9$. Likewise, in panel (b) we present the the area of the well S as a function of under the β . The trend is quadratic, $S(\beta) = s_0 + s_1\beta + s_2\beta^2$, with $s_0 = 2.2321$, $s_1 = -3.7433$ and $s_2 = 4.8112$. Figure obtained from Ref. [11].

We can obtain the analytic expression of $\tau = \tau(\beta)$ from Eq. 12 because the conserved value of ΔE must agree with the Eq. 8 when it is applied to a free moving particle. Then, we express $\tau(\beta)$ as

$$\tau(\beta) = \sqrt{3} \frac{(K_0 + K_1\beta + K_2\beta^2) - E_e}{s_0 + s_1\beta + s_2\beta^2}, \quad (13)$$

where we have expressed the value of the conserved energy of the system ΔE by $K_0 + K_1\beta + K_2\beta^2 - E_e$. Since the Eq. 13 is a fraction of two quadratic polynomials, it can be expressed as $\tau(\beta) = \Gamma_0 + \Gamma_1\beta + \Gamma_2\beta^2$, which corresponds to a quadratic polynomial as showed in Fig. 6. In Fig. 11 we compare the value of the parameter τ obtained from the numerical computations and the results from the analytic formula of Eq. 13.

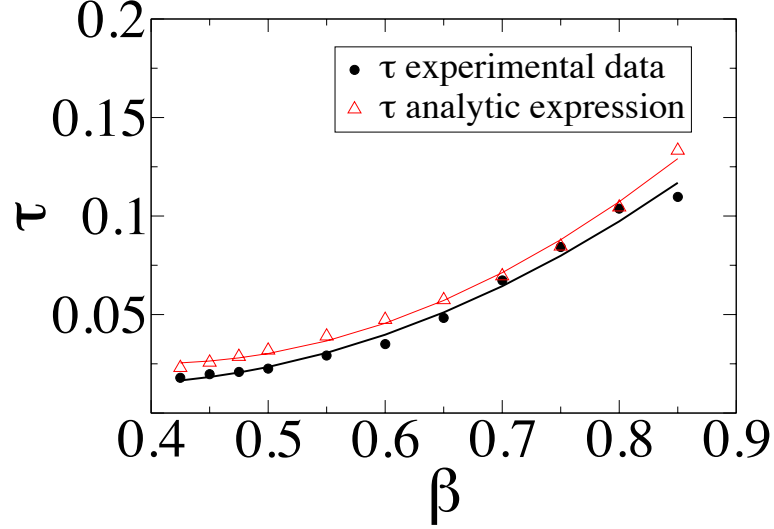


FIG. 11. (Color online) **Comparison between the data of the parameter τ from the numerical computations and the results obtained from the analytic expression** according to Eq. 13. Figure obtained from Ref. [11].

Now we will obtain a reasoning for the parameter α as a function of β according to the Eq. 6 in the open nonhyperbolic regime. Looking for that goal, we consider the stickiness effect of the KAM islands in the trajectories which leave the scattering region and eventually pass through the KAM tori. The basic idea is well explained in [24]. If a process that decays (or grows) exponentially is killed randomly, then the distribution of the killed state will follow a power law in one or both tails. Indeed, we can consider that all the particles leaving the scattering region follow an exponential decay law, but because some of the trajectories pass close to the KAM islands, then the exponential decay process is killed during a certain time. The average result is that the decay law when sizable KAM tori exist is algebraic. Therefore, if we consider the exponential decay law of the particles $P(t) = e^{-\tau t}$ killed at a random time T which is exponentially distributed with parameter ν , then the killed state $\bar{P} = e^{-\tau T}$ has the probability density function $f_{\bar{P}}(t) = (\frac{\nu}{\tau})t^{-\frac{\nu}{1-\tau}}$ for $t > 1$. Therefore, the average decay law of the particles shows a power law behavior. For the sake of clarity, τ is the parameter of Eqs. 12 and 13, which regulates the exponential decay law of the particles. When a particle trajectory passes close to a KAM island, then the KAM stickiness provokes that the escaping process is killed during a certain time. Indeed as we showed in Fig. 4, the higher the energy of the system is, the smaller the area of the KAM island is. Therefore, we can consider that for higher energies it is more difficult for a certain trajectory to pass close to the

KAM islands. The exponential decay of the particles is more probable to be killed at low energies than at higher energies. In that sense the parameter ν is directly related to the energy of the system so we can rewrite the expression of $f_{\bar{P}}(t)$ as a function of β as $f_{\bar{P}}(t) = \left(\frac{g(\beta)}{\tau}\right)t^{\frac{-g(\beta)}{1-\tau}}$. The function which relates ν to β is $g(\beta)$. Comparing $f_{\bar{P}}(t)$ with Eq. 6 we can write $\alpha(\beta) = \frac{g(\beta)}{1-\tau(\beta)}$.

We have proposed an expression for $g(\beta)$ that matches quite well the numerical values obtained for $\alpha(\beta)$ as

$$g(\beta) = \frac{1}{D_{PS}\sqrt{\Phi_{KAM}}},$$

where D_{PS} is the number of canonical coordinates defined on the phase space. In this case, $D_{PS} = 4$ since the canonical coordinates are $(x, y, p, q) \in \mathbb{R}^4$. According to the proposed expression, $g(\beta)$ is inversely proportional to the area of the KAM island due to the term $\frac{1}{\sqrt{\Phi_{KAM}}}$ and also to the dimension of the phase space. The higher the dimension of the phase space is, the less probable is for a particle to reach the KAM region since it has other directions where to go. The obtained formula to express the parameter α as a function of β is

$$\alpha(\beta) = \frac{1}{D_{PS}} \frac{\frac{1}{\sqrt{\Phi_{KAM}}}}{1 - \tau(\beta)}. \quad (14)$$

In Fig. 12 we compare the value of the parameter α obtained from the numerical computations and the results from the analytic formula of Eq. 14.

V. UNCERTAINTY DIMENSION

The *scattering functions* are one the most fundamental footprints of any chaotic scattering system. A scattering function relates an input variable of an incident particle with an output variable characterizing the trajectory of the particle, once the scattering occurs. These functions can be obtained empirically and, thanks to them, we can infer relevant information about the system. In Fig. 13, we can see a typical scattering function: the average escape time of a test particle *vs.* the initial shooting angle, for the relativistic Hénon-Heiles system. Red (dark gray) dots are the values of the escape times for a relativistic system with $\beta = 0.01$, while green (gray) dots denote the escape times for $\beta = 0.5$. We use two panels to represent the scattering function. The lower left panel shows the scattering function for a shooting angle $\phi \in [4.71, 6.71]$. The upper right panel is a magnification of the scattering function, varying the initial angle narrower, $\phi \in [5.35, 5.44]$. In order to obtain both panels, we shoot in both cases 1,000 particles from

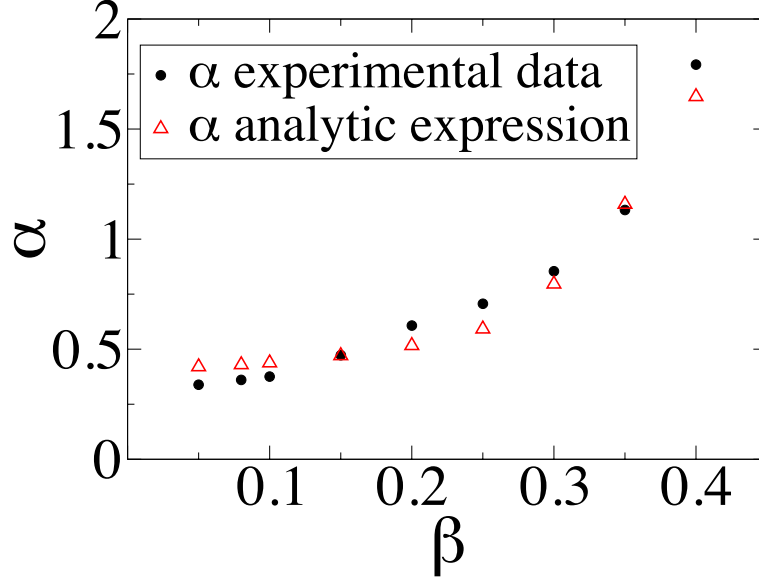


FIG. 12. (Color online) Comparison between the data of parameter α from the numerical computations and the results obtained from the analytic expression according to Eq. 14. Figure obtained from Ref. [11].

$(x, y) = (0, 1)$ into the scattering region with an initial velocity $v = 0.583$. In Fig. 13, we can see that the scattering function contains some regions where the escape time of the particle varies smoothly with the shooting angle. However, there are some other fractal regions with singularities, where a slightly different initial condition in the shooting angle implies an abrupt change in the particle escape time.

The crucial point is that, because, as we have seen in Fig. 13, any small variation in the neighborhood of a singular input variable implies a huge variation in the output variable, and furthermore, the range of variation of the output variable does not tend to zero despite the variation goes to zero. This type of behavior of the scattering function means that a small uncertainty in the input variable may make impossible any prediction about the value of the output variable. The fractal dimension D of the set of singular input variable values provides a quantitative characterization of the magnitude of such uncertainty. That is why the fractal dimension D is defined here as the uncertainty dimension. As it was previously demonstrated, when the regime of the chaotic scattering system is hyperbolic, all the orbits are unstable and then $0 < D < 1$. However, when the dynamics is nonhyperbolic, there are KAM islands in phase space and then $D \approx 1$ [25, 26].

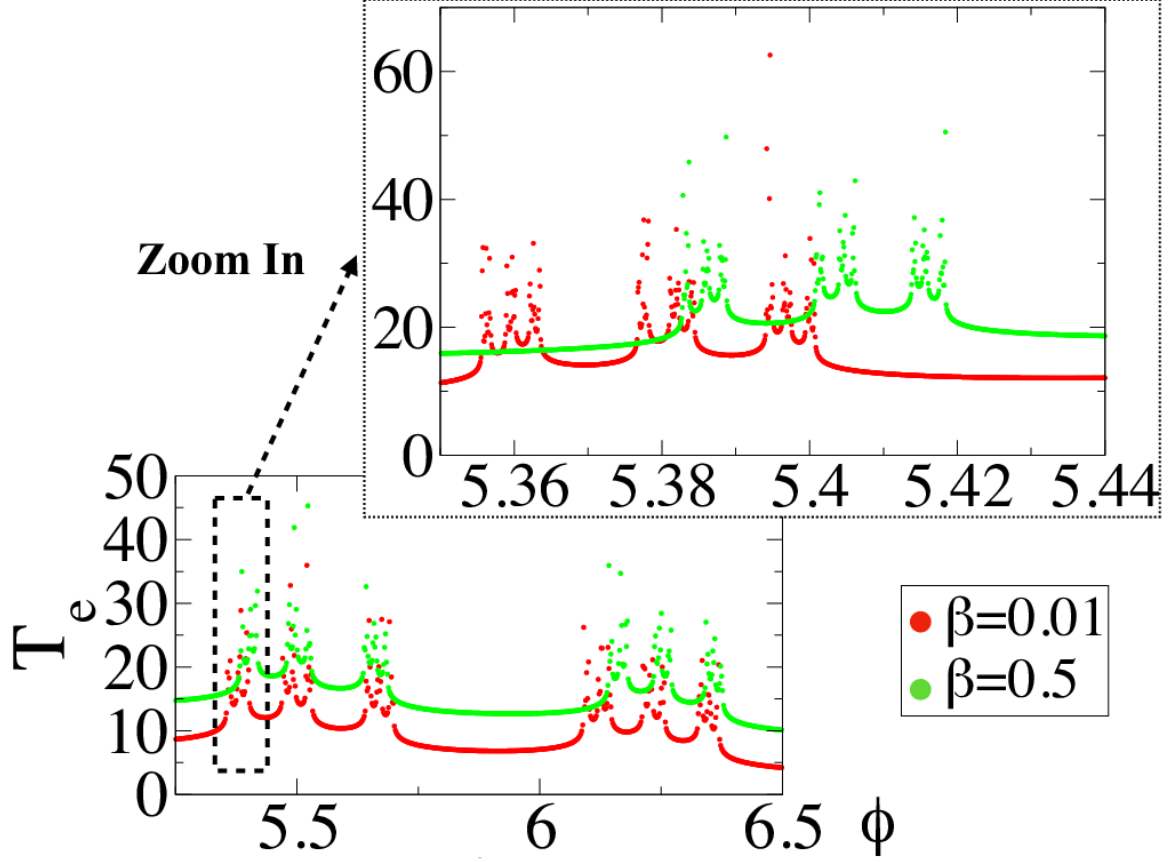


FIG. 13. (Color online) **Typical cattering function:** of the escape time T_e vs. the initial angle ϕ of 1,000 particles shot into the scattering region from $(x, y) = (0, 1)$ with initial velocity $v = 0.583$. Red (dark gray) dots represent the escape times for a relativistic system with $\beta = 0.01$, while green (gray) dots denote the escape time values for $\beta = 0.5$. The lower left panel shows the scattering function for a shooting angle $\phi \in [4.71, 6.71]$. Likewise, the upper right panel is a zoom-in of the scattering function, taking a narrower initial angle range, $\phi \in [5.35, 5.44]$. The scattering function contains some regions where the escape time of the particle varies smoothly with the shooting angle and, some others, where a slightly different initial condition in the shooting angle implies an abrupt change in the particle escape time. Figure obtained from Ref. [12].

In this section we investigate the evolution of the uncertainty dimension, D , in a typical scattering function as the parameter β is varied. In order to compute D , we use the uncertainty algorithm [27]. We select a horizontal line segment defined by $y_0 = 1$ from which we shoot the test particles towards the scattering region with initial velocity $v = 0.583$. For a certain initial

condition on the line segment, for instance $(x_0, y_0) = (0, 1)$, we choose a perturbed initial condition $(x_0, y_0) = (x_0 + \varepsilon, 1)$, where ε is the amount of perturbation. Then we let both trajectories evolve according to Eqs. 5. We track the time they last in the scattering region, and by which exit they escape. In case that the two trajectories escape from the scattering region at the same time or throughout the same exit, then we consider that both trajectories are *certain* with regard to the perturbation ε . Otherwise, we say both trajectories are *uncertain*. Taking a large number of initial conditions for each value of ε , we conclude that the fraction of uncertain initial conditions $f(\varepsilon)$ scales algebraically with ε as $f(\varepsilon) \sim \varepsilon^{1-D}$, or $f(\varepsilon)/\varepsilon \sim \varepsilon^{-D}$. Therefore, D is the uncertainty dimension. When we repeat this process for different values of β , we obtain the evolution of the uncertainty dimension D with β . As we can see in Fig. 14, $D \approx 1$ when $\beta \rightarrow 0$. Moreover, for $\beta \in [0, 0.625)$, there is a linear decrease of D with any increment in β . There is a crossover behavior at $\beta \approx 0.625$ such that for $\beta > 0.625$, the linear decrease of β is steeper.

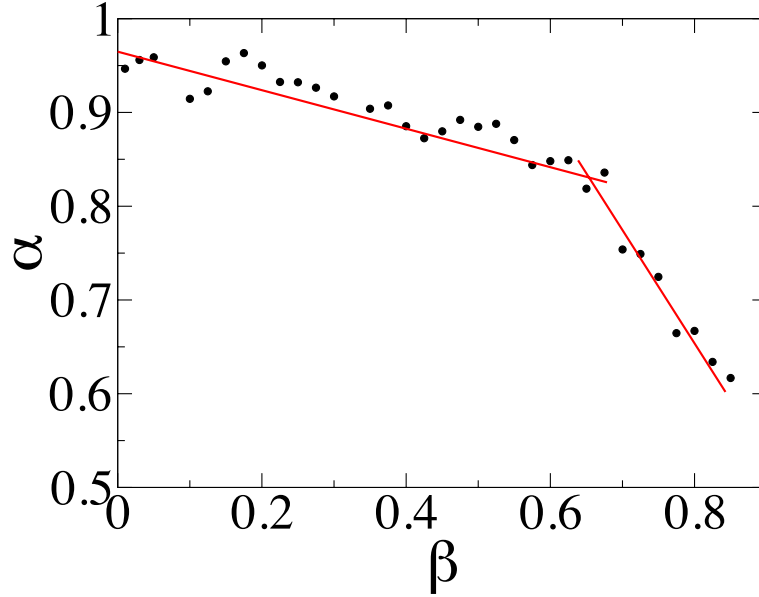


FIG. 14. (Color online) **Uncertainty dimension D** : evolution of the uncertainty dimension D in a scattering function defined on the horizontal initial line segment at $y_0 = 1$ with the variation of β . For many values of $\beta \in (0, 1)$ we randomly launch 1,000 test particles from the horizontal line segment passing through y_0 . The particles are shot towards the scattering region with initial velocity $v = 0.583$. The results indicate that $D \approx 1$ when $\beta \rightarrow 0$. Additionally, there is a linear decrease of D with any increment in β up to a value $\beta \approx 0.625$. At this point, there is a crossover behavior since, for values $\beta > 0.625$, there is a steeper linear decrease of β . Figure obtained from Ref. [12].

In order to provide a theoretical reasoning about the dependence of the uncertainty dimension D with the factor β , as shown in Fig. 14, we follow the approach explained in previous literature (see Ref. [28]). Firstly, as an informative example, we consider a Cantor set with a Lebesgue measure equals zero and a fractal dimension equals 1. We shall explain below why such a set is relevant to our construction. To construct this set, we proceed iteratively as follows. Iteration 1: starting with the closed interval $[0, 1]$ of the real numbers, we remove the open middle third interval. There are two remaining intervals of length $1/3$ each. Iteration 2: we remove the middle fourth interval from the two remaining intervals and, therefore, we have four closed intervals of length $1/9$. Iteration 3: again, we take away the fifth middle open interval from each four remaining intervals. Iteration n^{th} : there are $N = 2^n$ intervals, each of length $\epsilon_n = 2^{-n}[2/(n+2)]$. The total length of all the intervals is $\epsilon_n N \sim n^{-1}$ and it goes to zero as n goes to infinity. For covering the set by intervals of size ϵ_n , the required number of intervals is $N(\epsilon) \sim \epsilon^{-1}(\ln \epsilon^{-1})^{-1}$. On the other hand, the fractal dimension is $D = \lim_{\epsilon \rightarrow 0} [\ln(N(\epsilon))/\ln(\epsilon^{-1})]$, which clearly yields 1. We note that the exponent of the dependence $N(\epsilon) \sim 1/\epsilon^D$ is the uncertainty dimension D , as was previously defined. The weaker logarithmic dependence does not have any influence on the determination of the dimension. However, the logarithmic term is indeed the one that makes the Cantor set to be a Lebesgue measure zero since $\epsilon N \sim (\ln \epsilon^{-1})^{-1}$ tends to 0 as $\epsilon \rightarrow 0$. In order to generalize this example, we may consider that in each stage we remove a fraction $\eta_n = a/(n+b)$, where a and b are constants, from the middle of each of the 2^n remaining intervals. Then we find that

$$N(\epsilon) \sim (1/\epsilon)[\ln(1/\epsilon)]^{-a}. \quad (15)$$

According to Eq.(15), the slope at any point of the curve $\ln N(\epsilon)$ vs $\ln(1/\epsilon)$ is, by definition, $d \ln N(\epsilon)/d \ln(1/\epsilon)$, and it is always less than 1 for small ϵ , although it approaches 1 logarithmically as $\epsilon \rightarrow 0$. Therefore, the result about the fractal dimension is still $D = 1$.

Coming back to the relativistic chaotic scattering analysis, now we can do a parallelism with the fractal dimension of Cantor-like structures. First, we note that chaotic scattering occurs due to a nonattracting chaotic set (*i.e.*, a chaotic saddle) in phase space where the scattering interactions takes place [29]. Moreover, both the stable and the unstable manifolds of the chaotic saddle are fractals [30]. Scattering particles are launched from a line segment straddling the stable manifold of the chaotic saddle outside the scattering region. The set of singularities is the set of intersections of the stable manifold and the line segment, and it can be effectively considered a Cantor-like set.

There is an interval of input variables which leads to trajectories that remain in the scattering region for at least a duration of time T_0 . By time $2T_0$, there is a fraction η of these particles leaving the scattering region. In case that these particles are all located in the middle of the original interval, there are then two equal-length subsets of the input variable that lead to trajectories that remain in the scattering region for, at least, $2T_0$. Likewise, we may consider that a different fraction η of incident particles, whose initial conditions were located in the middle of the first two subintervals that remains at time $2T_0$, are now leaving the scattering region by $3T_0$. There are then four particle subintervals that remains in the scattering region for at least $3T_0$. If we continue this iterative procedure, we can easily recognize the parallelism of the emerging fractal structure made of the incident particles which never escape, and a Cantor-like set of zero Lebesgue measure. The fractal dimension D of the Cantor set then is given by

$$D = \frac{\ln 2}{\ln[(1 - \eta)/2]^{-1}}. \quad (16)$$

In the nonhyperbolic regime, the decay law of the particles is algebraic and this implies that the fraction η is not constant during the iterative process of construction of the Cantor set. At the n^{th} stage (being n large enough), the fraction η_n is approximately given by

$$\eta_n \approx -T_0 P^{-1} dP/dt \approx z/n. \quad (17)$$

This expression obviously yields a Cantor set with dimension $D = 1$ when we substitute $\eta_n \approx z/n$ in Eq.(16). If we compare this result with the mathematical construction of the Cantor set as described in Eq.(15), then we realize that the exponent z of the algebraic decay law corresponds to the exponent a of the Eq.(15). On the other hand, in the case of the hyperbolic chaotic scattering, the incident particles leave the scattering region exponentially. The exponent of the decay law τ is related with the fraction η as

$$\tau = T_0^{-1} \ln(1 - \eta)^{-1}. \quad (18)$$

Now, we are in the position to complete the reasoning behind the behavior of the uncertainty dimension D with the relativistic parameter β . As we pointed out in Sec. IV, the relation between the parameter τ of the hyperbolic regime and β follows a quadratic relation. Then, according to Eqs.(16) and (18) we may find that

$$D = \frac{\ln 2}{\ln 2 + T_0(\tau_0 + \tau_1\beta + \tau_2\beta^2)}. \quad (19)$$

According to Eq.(19), the fractal dimension D is always less than 1 and it decreases while β increases. In the limit, as $\beta \rightarrow 1$, the quadratic relation between the particles decay rate τ and β is no longer valid, since the kinetic energy of the system grows to $+\infty$. In that case, as $\beta \rightarrow 1$, then $\tau \rightarrow +\infty$ and, therefore, $D \rightarrow 0$. Likewise, the exponent α of the algebraic decay law and the parameter β are also related in a quadratic manner too. Then if we take into consideration Eqs.(16) and (17) we obtain

$$D = \frac{\ln 2}{\ln\left(\frac{2}{1-A_0+A_1\beta+A_2\beta^2}/n\right)}. \quad (20)$$

As $\beta \rightarrow 0$, we have $D \rightarrow 1$ for large n , and, moreover, we find that $dD/d\beta = 0$ since we recover the Newtonian system. When β increases, then D decreases. For large values of n , the value of $1 - (Z_0 + Z_1\beta + Z_2\beta^2)/n$ is always larger than 0 and smaller than 1 because the maximum value of z is $z \approx 1.5$, as we noted in Sec. II. Despite the KAM destruction, the transition from the algebraic regime to the hyperbolic one is not very abrupt. This is the reason why the uncertainty dimension D decreases smoothly with β as shown in Fig. 14 up to $\beta \approx 0.625$. When we reach this value, the hyperbolic regime is clear and it yields a steeper change in D vs. β .

VI. EXIT BASINS DESCRIPTION

A. Exit basins description

We define *exit basin* as the set of initial conditions whose trajectories converges to an specified exit [31]. Likewise, an initial condition is a *boundary point* of a basin B if every open neighborhood of y has a nonempty intersection with basin B and at least one other basin. The *boundary* of a basin is the set of all boundary points of that basin. The basin boundary could be a smooth curve, but in chaotic systems, the boundaries are usually fractal. In this case, since the phase space resolution is finite in any real physical situation, those fractal structures impose an extreme dependence on the initial conditions, which obstructs the prediction of the system final state. For that reason, the understanding of the exit basin topology is crucial to foresee the final fate of the system. In this section, we will provide a qualitative description of how the exit basins of the

Hénon-Heiles system evolve while the ratio β is increased.

We use Poincaré section surfaces (q, y) at $t = 0$ and $x = 0$ to represent the exit basins. To carry out our simulations, we shoot 1,000,000 particles from $x = 0$ and $y \in [-1, 1]$, with initial angles $\phi \in [0, \pi]$. Then, we follow each trajectory and we register by which exit the particles have escaped from the scattering region. If a particle leaves the scatterer by Exit 1, then we color the initial condition, (q_0, y_0) , in brown (gray). Likewise, we color the initial condition in blue (dark gray) if the particle escapes by Exit 2 and, in case it leaves the scatterer by Exit 3, we color it in yellow (light gray). When a particle remains in the scattering region after t_{max} , then we color its initial condition in black. We have run different simulations to plot the exit basins of the Hénon-Heiles system for a wide range of parameters β , as shown in Fig. 15.

In Figs. 15(a-e), we can see the evolution of the exit basins of the Hénon-Heiles system while the parameter β is increased. In Fig. 15(a), we represent the Newtonian case. It corresponds to $E_N = 0.17$, which is fairly close to the escaping energy threshold value $E_e = 1/6$. At this energy, the exit basins are quite mixed throughout the phase space and there are many initial conditions (black dots) which do not escape from the scattering region. Likewise, the KAM islands can be easily recognized as the black areas inside the phase space. In Fig. 15(b), we can see the relativistic effects of the Lorentz corrections for $\beta = 0.2$. The exit basins are still quite mixed although now there are larger regions where we can see compact exit basins. In Fig. 15(c), we represent the exit basins of the system for $\beta = 0.4$. The exit basins are clearly located in regions and their boundaries are fractal. There are still some portions of the phase space where the basins corresponding to Exits 1, 2 and 3 are mixed. However, the KAM islands are destroyed and there are just a few trajectories remaining in the scattering region after T_{max} (colored in black). Figure 15(d) represents the exit basins of the system for $\beta = 0.625$. There are no regions where the exit basins are mixed. The boundaries are fractal. Lastly, in Fig. 15(e), we show the Hénon-Heiles exit basins for $\beta = 0.9$. The exit basins are smoothly spread on the phase space and the fractality of the boundaries has decreased.

Many dynamical system of interest, with two or more coexisting attractors (or escapes), exhibit a singular topological property in their basin boundaries that is called the *property of Wada* [32] here. If for every boundary point u_b of a certain basin, we can find an infinitely tiny open neighborhood centered in u_b that contains points from the rest of the basins, we can say that this boundary

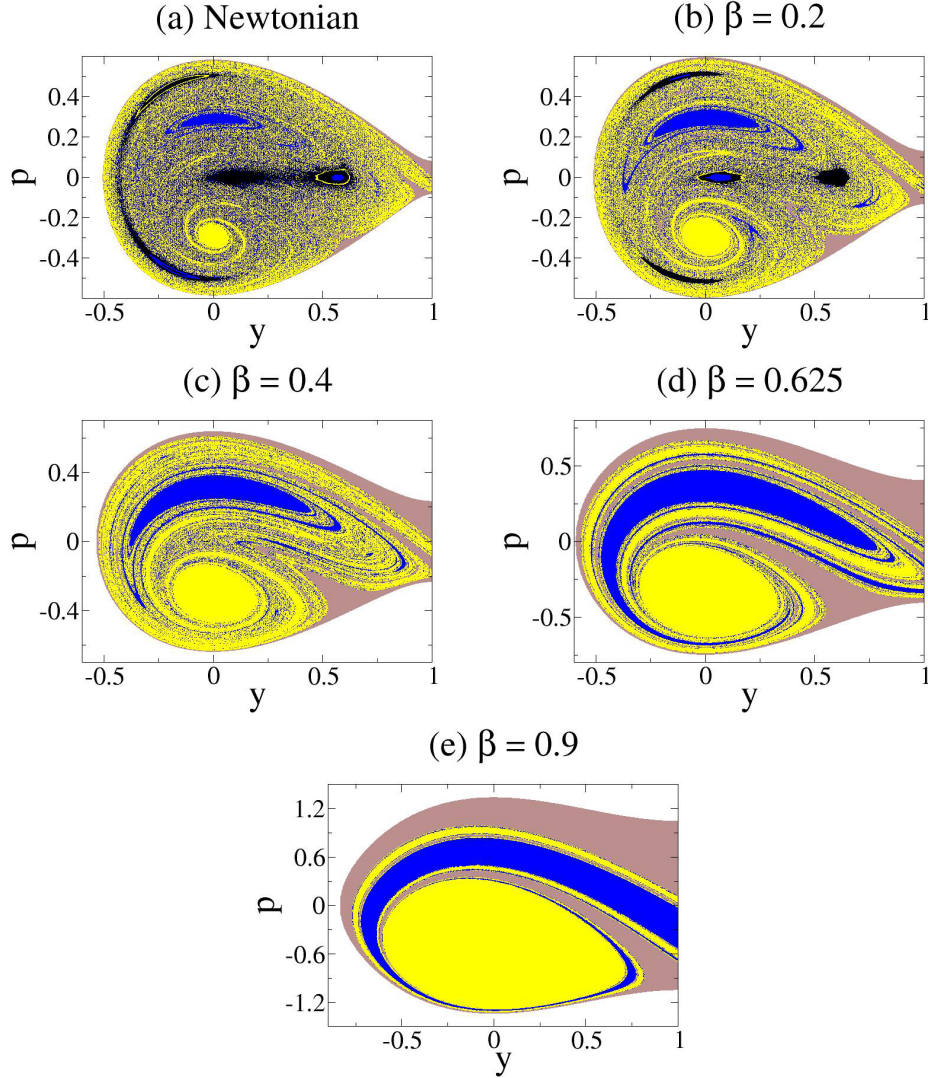


FIG. 15. (Color online) **Evolution of the exit basins of the Hénon-Heiles system for different values of β .** The sets of brown (gray), blue (dark gray) and yellow (light gray) dots denote initial conditions resulting in trajectories that escape through Exits 1, 2 and 3 (see Fig. 1), respectively. The black regions denote the KAM islands and, generally speaking, the black dots are the initial conditions which do not escape. (a) Newtonian case: the exit basins are quite mixed throughout the phase space and the KAM islands can be easily recognized as the big black regions inside phase space. (b) $\beta = 0.2$: the exit basins are still fairly mixed. The regions corresponding to exit basins are larger than in the Newtonian case. (c) $\beta = 0.4$: exit basin regions are larger. The exit basin boundaries are fractal. The KAM islands are destroyed. (d) $\beta = 0.625$: the exit basins are not mixed anymore. The boundaries are fractal. (e) $\beta = 0.9$: the boundaries are smoother, and the exit basins occupy a larger region of phase space. Figure obtained from Ref. [12].

has the property of Wada. A logical consequence of this definition is that a Wada basin boundary is the same boundary for all the basins. The property of Wada is a very interesting characteristic because the fate of any dynamical system is harder to predict since we cannot foresee a priori by which of the exits any initial condition close to the boundaries is going to escape. In that case, the degree of unpredictability of the destinations can be more severe than the case where there are just fractal basins with only two potential destinations associated. In the energy regime that we are considering, the Hénon-Heiles system exhibits three symmetric exits to escape from the scattering region, giving rise to three qualitatively distinct scattering destinations. This allows Wada basin boundaries to occur. Each exit of the system has its own associated exit basin. Previous research described some algorithms to obtain the numerical verification of the Wada property in dynamical systems [33–36]. In this paper, we resort to the appearance of the exit basin boundaries to give visual indications about the persistence of the Wada property as the parameter β is varied. For values of $\beta \leq 0.625$, we have observed that the boundary points of any exit basin magnification seem to be surrounded by points from the three basins. However, when $\beta > 0.625$, we have seen that the boundary points are exclusively surrounded by points belonging just to two basins. In order to give visual examples, we show Figs. 16(a) and (b). Both are detailed analysis of the Hénon-Heiles exit basins for $\beta = 0.625$ and $\beta = 0.9$, respectively, when we perform the computations on a tiny portion of the exit basins, in $y \in [-0.001, 0.001]$. Therefore, Fig. 16(a) is a zoom-in of the Fig. 15(d) and Fig. 16(b) is a zoom-in of the Fig. 15(e). For $\beta > 0.625$, the exit basin representations are similar to the one described in Fig. 16(b), where we can observe that, for example, the boundary located at $p = 1$ is smooth. Moreover, this boundary divides only two basins, the one corresponding to Exit 1 (brown–gray–) from the one associated to Exit 3 (yellow–light gray–). This is a visual indication that the Wada property might not be observable in the relativistic Hénon-Heiles system for $\beta > 0.625$; at least, at the numerical scale we have performed the calculations. In that sense, we may suppose that the unpredictability associated to the final destination of the trajectories for values of $\beta \leq 0.625$ is higher.

As we can see, considerations of special relativity have qualitative implications on the exit basin topology of the system, even for low values of β . In the following sections we will provide more insights about this statement from a quantitative point of view.

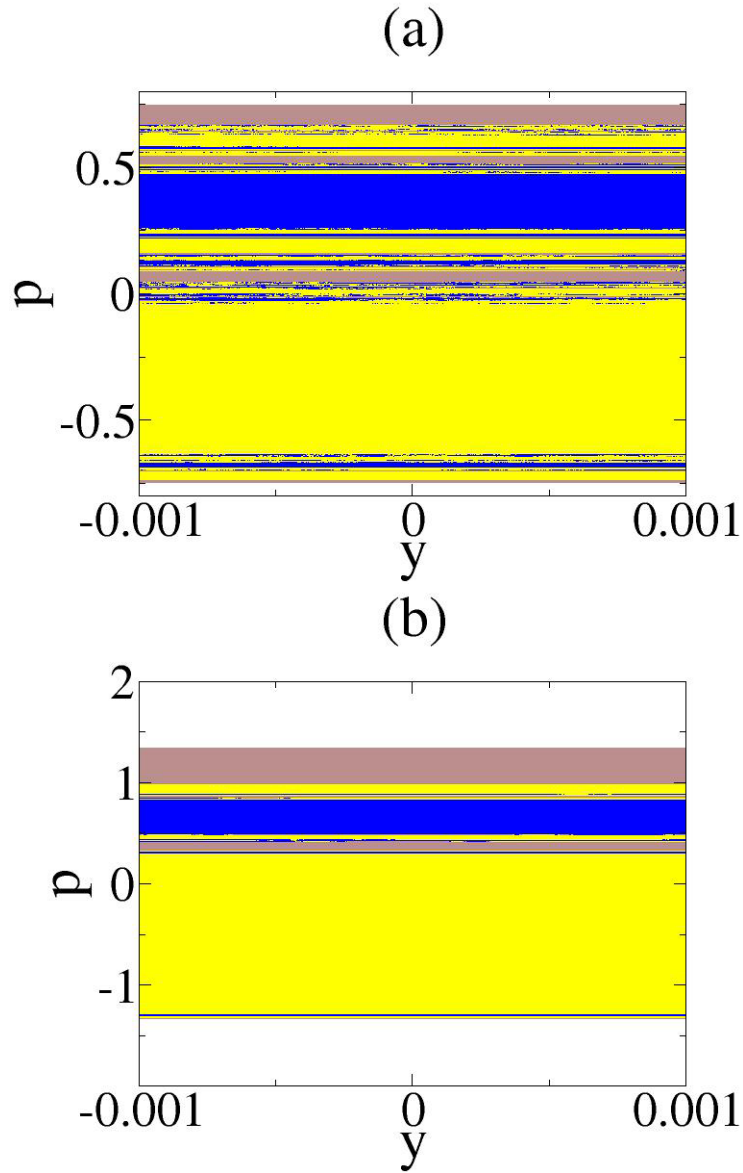


FIG. 16. (Color online) **Zoom-in of the exit basins for $\beta = 0.625$ and $\beta = 0.9$.** The sets of brown (gray), blue (dark gray) and yellow (light gray) dots denote initial conditions resulting in trajectories that escape through Exits 1, 2 and 3 (see Fig. 1), respectively. In (a) we can see that the boundary points seem to be surrounded by points from other basins. Nonetheless, in (b) we can find boundary points which are surrounded only by points of just two basins. The boundary located at $p = 1$ is smooth and it divides just two basins, the one corresponding to Exit 1 from the corresponding to the Exit 3. Figure obtained from Ref. [12].

B. Basin entropy

The *basin entropy* is a novel tool developed to quantitatively describe the exit basin topology of any dynamical system [37]. The main idea behind the concept of basin entropy is that the continuous phase space of the system can be considered a discrete grid due to the finite resolution of any experimental or numerical procedure to determine any point in phase space. In fact, this unavoidable scaling error indeed does induce wrong predictions in chaotic systems even when they are completely deterministic. Therefore, the basin entropy helps to quantify to what extent one system is chaotic according to the topology of its phase space. In particular, considering the exit basins of the Hénon-Heiles system as the ones shown in Fig. 5, we can easily create a discrete grid if we assume a finite precision δ in the determination of the initial conditions and we cover the phase space with boxes of size δ . This way, every piece of the grid is surrounded by other pieces, and we may define a *ball* around a piece as the pieces sharing some side with it. The method to calculate the basin entropy considers that, the ball is a random variable, being the potential results of that variable the different exit basins. Taking into account that the pieces inside the ball are independent and applying the Gibbs entropy concept, the basin entropy S_b is defined as

$$S_b = \sum_{k=1}^{k_{max}} \frac{N_k^0}{N^0} \delta^{\alpha_k} \log(m_k), \quad (21)$$

where k is the label for the different exit basin boundaries, m_k is the number of exit basins contained in a certain ball and α_k is the uncertainty dimension of the boundary k as defined in Sec. V. The ratio $\frac{N_k^0}{N^0}$ is a term related with the portion of the discretized phase space occupied by the boundaries, that is, the number of pieces lying in the boundaries divided by the total number of pieces in the grid. Therefore, there are three sources that increase the basin entropy: (a) $\frac{N_k^0}{N^0}$, that is, the larger portion of the phase space occupied by the boundaries, the higher S_b ; (b) the uncertainty dimension term δ^{α_k} , related to the fractality of the boundaries; (c) $\log(m_k)$, which is a term related to the number of different exit basins m_k . In the case that the basins exhibit the property of Wada, then there is just one boundary that separates all the basins. In this case, the term $\log(m_k)$ is maximum and S_b is increased because all the possible exits are present in every boundary box. As we have shown in Sec. VI, this may be the case for the relativistic Hénon-Heiles system for $\beta \leq 0.625$.

In Fig. 17, we can see the evolution of the basin entropy S_b of the Hénon-Heiles system with

β . We can distinguish 4 regions: (A) $\beta \in (0, 0.2]$, increasing of S_b up to $\beta \approx 0.2$; (B) $\beta \in [0, 0.4]$, steep decrease of S_b until $\beta \approx 0.4$; (C) $\beta \in (0.4, 0.625]$ and (D) $\beta \in (0.625, 0.9)$, smoother decrease of S_b . As was shown in Sec. V, the uncertainty dimension α is a monotonically decreasing function, so the increase of S_b in the region (A) can only be explained because of a higher increase of $\frac{N_1^0}{N^0}$. In region (A), when β is increased, the zones where the basins are mixed are indeed reduced. However, the KAM islands are reduced. These effects can be seen in the exit basin evolution from Fig. 5(a) to Fig. 5(b). Moreover there are more pieces in the grid of the discretized phase space occupied by the boundaries. In the region (B) there is an important decrease of S_b because of the reduction of $\frac{N_1^0}{N^0}$. In this region, while β is increased, the areas of the phase space where the basins are mixed are negligible and the KAM islands are progressively losing relevance in phase space. At $\beta \approx 0.4$ there is an inflection point, just when the KAM islands are destroyed. There are fewer pieces of the grid occupied by the boundaries. In the region (C), $\beta \in (0.4, 0.625]$, the exit basin areas are larger and they grow as β increases, while the fractality of the boundaries decreases. This is exactly what was found in Fig. 4, where the uncertainty dimension α decreases abruptly from $\beta \approx 0.625$ on. In region (D), the fractality of the boundaries is reduced and there have been some visual indications about the disappearance of the Wada basins, as described in Sec. VI.

As we have seen in the course of this work, the exit basin topology of the relativistic Hénon-Heiles varies with β , even for low velocities. From this point of view, the properties of the system that depend on the phase space topology may vary too.

VII. APPLICATIONS TO NATURAL PHENOMENA

We have seen along this work that the dynamics of the relativistic Hénon-Heiles mainly depends on the evolution of the topology of the phase space when we vary β . In particular, we have concluded that the existence of KAM islands in the phase space of the system is the key driver to exhibit a nonhyperbolic or a hyperbolic dynamics. From this point of view, the global properties of the system which depend on the topology of the phase space may vary even for low velocities. Although the Hénon-Heiles potential was initially developed to model the motion of stars around an axisymmetrical galaxy, we think that the phenomena described in the present work may be related to many other phenomena occurred in Nature. For instance, the M-sigma (or M- σ) relation is an empirical correlation between the stellar velocity dispersion σ of a galaxy bulge and

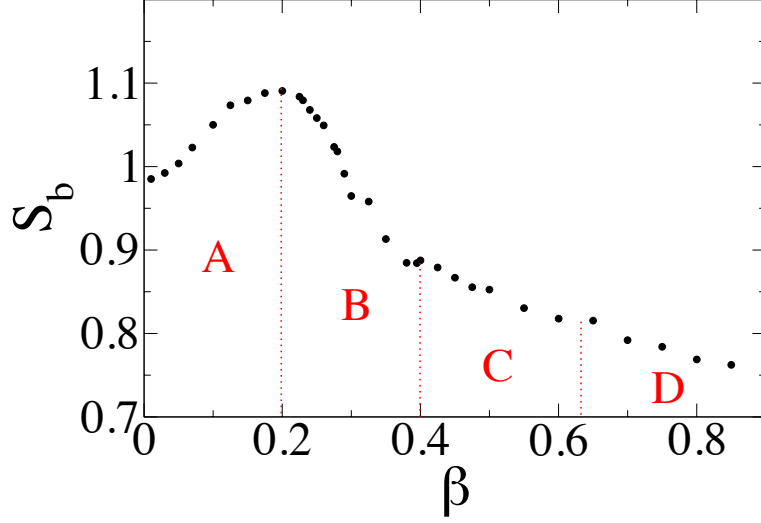


FIG. 17. (Color online) **Evolution of the basin entropy S_b of the relativistic Hénon-Heiles system with β .** There are represented 4 regions: (A) $\beta \in (0, 0.2]$, increase of S_b up to $\beta \approx 0.2$; (B) $\beta \in [0, 0.4]$, steep decrease of S_b until $\beta \approx 0.4$; (C) $\beta \in (0.4, 0.625]$ and (D) $\beta \in (0.625, 0.9)$, both regions show a smoother decrease of S_b . The behavior of S_b in region (A) is explained because of the reduction of both the KAM islands and the regions where the basins are mixed. The global effect is that $\frac{N_1^0}{N^0}$ is increased. In contrast, in region (B) the areas where the basins are mixed are negligible and the KAM islands are rapidly tinnier. These effects cause a relevant reduction of $\frac{N_1^0}{N^0}$. In regions (C) and (D) the exit basin sets are progressively larger and smoother (as was shown in Fig. 5). Figure obtained from Ref. [12].

the mass M of the supermassive black hole at its center (see Refs. [38, 39]). This correlation is quite relevant since it is commonly used to estimate black hole masses in distant galaxies using the easily measured quantity σ . The M -sigma relation is well described by an algebraic power law and, although the applications of the Hénon-Heiles and the M -sigma models are very different, we speculate that the underlying mathematical properties are similar, including the presence of KAM islands in the phase space of both systems. Therefore, the KAM islands would be responsible of the algebraic decay law and, hypothetically, their destruction would imply an exponential decay law to relate σ with the mass M of the supermassive black hole.

Examples of systems that can be described by the Hénon-Heiles Hamiltonian are, for instance, the planar three-body system, buckled beams and some stationary plasma systems [40]. One relevant topic of special interest that is also modeled by the Hénon-Heiles Hamiltonian is the dynamics

of charged particles in a magnetic dipole field (which is also called the Störmer problem). Since a long time, scientists have studied it in the context of the northern lights and cosmic radiation and it models how a charged particle moves in the magnetic field of the Earth. The analysis of this system leads to the conclusion that charged particles are trapped in the Earth magnetosphere or escape to infinity, and the trapping region is bounded by a torus-like surface, the Van Allen inner radiation belt. In the trapping region, the motion of the charged particles can be periodic, quasi-period or chaotic [41]. According to the research we have presented in this chapter, if we want to study global properties of the Störmer problem, we should consider the relativistic effects because those properties depend on the exit basin topology. In those cases, we may expect that the uncertainty associated to the prediction of the final state of the particles varies as the parameter β increases.

VIII. CONCLUSIONS

In the last years, there has been an important progress in understanding the relativistic effects in chaotic scattering. Most of the research has been focused on studying the discrepancies between the Newtonian and the relativistic approaches over the trajectories of the particles. Here we show that some global relevant properties of chaotic scattering systems, do depend on the effect of the Lorentz transformations and we may consider the relativistic corrections in case we want to describe them in a realistic manner, even for low velocities. We have used the Hénon-Heiles system in order to undertake our theoretical reasoning and to perform the numerical computations.

We consider the global properties of the Hénon-Heiles system vary because the Lorentz corrections destabilize the topology of the phase space. In that sense, according to the regime of energies we have chosen for our numerical calculations, the KAM islands are fully destroyed for $\beta \approx 0.4$. We have proved in Fig. 3 that the average escape time \bar{T}_e of the Hénon-Heiles system decreases when β increases. Indeed at $\beta \approx 0.4$ there is a leap where the linear trend of \bar{T}_e changes abruptly. This can be easily explained from the perspective of the KAM islands destruction (see Fig. 4). We have explained the shape of the curves $\bar{T}_e(\beta)$, $\alpha(\beta)$ and $\tau(\beta)$ in Figs. 3, 5 and 6 by energetic considerations. We have also characterized the decay laws of the open-nonhyperbolic and hyperbolic regimes, obtaining algebraic expressions that fits the data from our numerical computations.

We have also focused our attention in describing different characteristics of the exit basing topology as the uncertainty dimension, the Wada property and the basin entropy of the relativistic Hénon-Heiles system. We have found that the Lorentz corrections modify these properties. We have shown in Fig. 13 the evolution of the uncertainty dimension, D , in a typical scattering function as the parameter β is varied. We found that D decreases almost as β increases up to a certain value of the parameter $\beta \approx 0.625$, when a crossover phenomenon occurs and D decreases abruptly. This takes place due to the transition from the algebraic particles decay law to the exponential decay law. We have also described in a qualitative manner the evolution of the exit basin topology with the parameter β (see Fig. 15). Moreover, we have found a qualitative evidence that the Wada basin boundaries disappear for $\beta > 0.625$. Lastly, we have used the concept of basin entropy to quantify the evolution of the exit basins with any variations of the parameter β (see Fig. 17). All our results point out that the uncertainty in the prediction of the final fate of the system depends on the considered value of β , and this relation is not linear. There are some intervals, *i.e.*, $\beta \in (0, 0.2]$, where the S_b is increased as β grows, whereas there are some others, *i.e.*, $\beta \in (0.4, 0.625]$, where the S_b decreases rapidly.

As we have seen, if we want to make accurate predictions about the final state of any chaotic scattering system, we think that the relativistic corrections should always be considered, regardless the energy of the system.

Lastly, we have speculated about the possibility of finding this dependence of the global properties of the system with the topology of the phase space in many other phenomena in Nature. For instance, the M - σ correlation is well described by an algebraic power law. We may consider that this relation is due to the presence of KAM islands in the phase space. Its destruction would involve an exponential decay law. Another example of the application to real problems in Nature of the results that we have obtained is, for example, the description of the dynamics of charged particles moving through a magnetic dipole-field as the one modeled by the Störmer problem. Therefore, we consider that our results are useful for a better understanding of the relativistic chaotic scattering systems.

IX. ACKNOWLEDGMENTS

We dedicate this work to our colleague and friend Valentin Afraimovich. This work was supported by the Spanish State Research Agency (AEI) and the European Regional Development Fund (FEDER) under Project No. FIS2016-76883-P. MAFS acknowledges the jointly sponsored financial support by the Fulbright Program and the Spanish Ministry of Education (Program No. FMECD-ST-2016).

- [1] J. M. Seoane and M. A. F. Sanjuán. Rep. Prog. Phys **76**, 016001 (2012).
- [2] E. Ott and T. Tél. Chaos **3**, 4 (1993).
- [3] C. Grebogi, E. Ott, and J.A. Yorke. Physica D **7**, 181 (1983).
- [4] T. Tél, B. L. Hao (Ed.), *Directions in Chaos*, Vol. 3, edited by B. L. Hao (World Scientific, Singapore, 1990), p. 149; in *STATPHYS 19*, edited by B. L. Hao (World Scientific, Singapore, 1996), p.243.
- [5] H. C. Ohanian, *Special Relativity: A Modern Introduction* (Physics Curriculum & Instruction, USA, 2001).
- [6] B. L. Lan. Chaos **16**, 033107 (2006).
- [7] B. L. Lan. Chaos, Solitons & Fractals **42**, 534 (2009).
- [8] B. L. Lan and F. Borondo. Phys. Rev. E **83**, 036201 (2011).
- [9] S-N Liang, B. L. Lang. Results in Physics **4**, 187 (2014).
- [10] J. M Aguirregabiria. arXiv: 1004.4064v1 (2010).
- [11] J. D. Bernal, J. M. Seoane and M. A. F. Sanjuán. Phys. Rev. E **95**, 032205 (2017).
- [12] J. D. Bernal, J. M. Seoane and M. A. F. Sanjuán. Phys. Rev. E **97**, 042214 (2018).
- [13] J. D. Bernal, J. M. Seoane and M. A. F. Sanjuán. Phys. Rev. E **88**, 032914 (2013).
- [14] M. Hénon and C. Heiles. Astron. J. **69**, 73 (1964).
- [15] R. Barrio, F. Blesa, and S. Serrano. Europhys. Lett. **82**, 10003 (2008).
- [16] G. Contopoulos. Astron. Astrophys. **231**, 41 (1990).
- [17] J. M. Seoane and M. A. F. Sanjuán. Phys. Lett. A **372**, 110 (2008).
- [18] J. M. Seoane, L. Huang, M. A. F. Sanjuán, and Y.-C. Lai. Phys. Rev. E **79**, 047202 (2009).
- [19] J. M. Seoane and M. A. F. Sanjuán. Int. J. Bifurcation and Chaos **20**, 2783 (2010).

- [20] C. F. F. Karney. *Physica D* **8**, 360 (1983); B. V. Chirikov and D. L. Shepelyansky. *Physica D* **13**, 395 (1984); J. Meiss and E. Ott. *Physica D* **20**, 387 (1986); Y.-C. Lai, M. Ding, C. Grebogi, and R. Blümel. *Phys. Rev. A* **46**, 4661 (1992).
- [21] M. Ding, T. Bountis and E. Ott. *Phys. Lett. A* **8**, 395 (1991).
- [22] H. J. Zhao and M. L. Du. *Phys. Rev. E* **76**, 027201 (2007).
- [23] M. C. Gutzwiller. *Chaos in Classical and Quantum Mechanics* (Springer, New York, 1990).
- [24] W. J. Reed and B. D. Hughes. *Phys. Rev. E* **66**, 067103 (2002).
- [25] Y.-T. Lau, J. M. Finn and E. Ott. *Phys. Rev. Lett.* **66**, 978 (1991).
- [26] S. Bleher, E. Ott and C. Grebogi. *Phys. Rev. Lett.* **63**, 919 (1989).
- [27] C. Grebogi, S. W. McDonald, E. Ott and J. A. Yorke. *Phys. Lett. A* **99**, 415 (1983).
- [28] J. M. Seoane, M. A. F. Sanjuán and Y.-C. Lai. *Phys. Rev. E* **76**, 016208 (2007).
- [29] S. Bleher, E. Ott and C. Grebogi. *Phys. Rev. Lett.* **63**, 919 (1989); S. Bleher, C. Grebogi and E. Ott. *Physica D* **46**, 87 (1990).
- [30] C. Grebogi, S. W. McDonald, E. Ott and J. A. Yorke. *Phys. Lett. A* **99**, 415 (1983); S. W. McDonald, C. Grebogi, E. Ott and J. A. Yorke. *Phys. Lett. D* **17**, 125 (1985).
- [31] G. Contopoulos. *Order and Chaos in Dynamical Astronomy*. (Springer, New York, 2002).
- [32] J. Kennedy and J. A. Yorke. *Phys. D* **51**, 213 (1991).
- [33] H. E. Nusse and J. A. Yorke. *Physica D* **90**, 242 (1996);
- [34] J. Aguirre, J. C. Vallejo and M. A. F. Sanjuán. *Phys. Rev. E* **64**, 066208 (2001);
- [35] J. M. Seoane, J. Aguirre, M. A. F. Sanjuán and Y.-C. Lai. *Chaos* **16**, 023101 (2006);
- [36] A. Daza, A. Wagemakers, Miguel A. F. Sanjun and J. A. Yorke. *Sci. Rep.* **5**, 16579 (2015);
- [37] A. Daza, A. Wagemakers, B. Georgeot, D. G.-Odelin and M. A. F. Sanjuán. *Sci. Rep.* **6**, 31416 (2016).
- [38] F. Ferrarese and D. Merritt. *The Astrophysical Journal*, **539** (2000).
- [39] K. Gebhardt, R. Bender, G. Bower, A. Dressler, S. M. Faber, A. V. Filippenko, R. Green, C. Grillmair, L. C. Ho, J. Kormendy, T.R. Lauer, J. Magorrian, J. Pinkney, D. Richstone, S. Tremaine. *The Astrophysical Journal* **539** (2000).
- [40] J. C. Bastos, C. G. Ragazzo and C. P. Malta. *Phys. Lett. A* **241**, 35 (198).
- [41] R. Dilao and R. Alves-Pires. *Chaos in the Störmer Problem. Progress in Nonlinear Differential Equations and Their Applications*. (Birkhäuser Verlag Basel, Switzerland, 2008).